Observation of water dangling OH bonds around dissolved nonpolar groups

P. N. Perera[a], K. R. Fega[a], C. Lawrence[b], E. J. Sundstrom[a], J. Tomlinson-Phillips[a], and Dor Ben-Amotz[a,1]

[a]Department of Chemistry, Purdue University, West Lafayette, IN 47907; and [b]Department of Chemistry, Grand Valley State University, Allendale, MI 49401

Edited by Michael D. Fayer, Stanford University, Stanford, CA, and approved June 12, 2009 (received for review April 3, 2009)

We report the experimental observation of water dangling OH bonds in the hydration shells around dissolved nonpolar (hydrocarbon) groups. The results are obtained by combining vibrational (Raman) spectroscopy and multivariate curve resolution (MCR), to reveal a high-frequency OH stretch peak arising from the hydration shell around nonpolar (hydrocarbon) solute groups. The frequency and width of the observed peak is similar to that of dangling OH bonds previously detected at macroscopic air–water and oil–water interfaces. The area of the observed peak is used to quantify the number of water dangling bonds around hydrocarbon chains of different length. Molecular dynamics simulation of the vibrational spectra of water molecules in the hydration shell around neopentane and benzene reveals high-frequency OH features that closely resemble the experimentally observed dangling OH vibrational bands around neopentyl alcohol and benzyl alcohol. The red-shift of ≈50 cm^{-1} induced by aromatic solutes is similar to that previously observed upon formation of a π-H bond (in low-temperature benzene–water clusters).

hydrophobic | interface | vibration | Raman

Changes in the structure and dynamics of water induced by nonpolar groups have long been considered to play a key role in protein folding, ligand binding, and the formation of biological cell membranes (1). Early thermodynamic evidence suggested that water may form an "iceberg" or clathrate-like structure around nonpolar molecules (2). Although no such rigid structures are currently thought to form (3), recent experimental (4, 5) and theoretical (6) results indicate that the rotational mobility of water molecules is reduced around nonpolar solutes (relative to bulk water). Moreover, fundamental theoretical arguments (and simulation measurements) imply that the size of a hydrophobic group may play a critical role in dictating water structure (7). This has led to the provocative suggestion that the structure of water around hydrophobic groups of nanometer (or greater) size may bear some resemblance to that at a macroscopic air–water interface (8). Although cohesive interactions between water and nonpolar groups tend to suppress the formation of an interfacial vapor layer (8–11), recent experimental (and molecular dynamics) studies indicate that the nonpolar binding cavity in bovine β-lactoglobulin is completely dehydrated in liquid water (12). Moreover, both experimental and simulation evidence suggests that water at nonpolar interfaces experiences significantly larger fluctuations than either bulk water or water at hydrophilic interfaces (13, 14). Here, we present experimental evidence that reveals a similarity between the structure of water around dissolved hydrocarbon groups and that at macroscopic oil–water interfaces (15–18), in the sense that both interfaces induce the formation of dangling OH bonds.

We have detected water dangling OH bonds by combining vibrational Raman spectroscopy with multivariate curve resolution (MCR). This procedure is used to decompose solution spectra into bulk water and solute-correlated spectral components—the latter of which includes hydration-shell vibrational features. Although, MCR is a well-established method for quantifying mixture compositions (by using spectroscopic and/or chromatographic data) (19), we have recently used this method to measure solvation-shell spectra (20), and here, we employ it to uncover dangling OH vibrational bands arising from the hydration shells around dissolved nonpolar groups.

The remainder of this article begins by describing the results of the experiments we performed to confirm our assignment of the observed peak to water dangling OH bonds. Changes in the intensity of the dangling OH peak are then used to estimate the number of water dangling OH bonds around hydrocarbon chains of different size. The width of the observed dangling OH peak is used to establish a lower bound on the lifetime of the associated hydration-shell structure. Observed differences between the average force along the dangling OH bond induced by saturated (alkane) and unsaturated (aromatic) hydrocarbon groups are shown to be consistent with molecular dynamics simulation predictions and previous experimental studies of π-H bonding in benzene–water clusters. Experimental and simulation details are provided in *Materials and Methods*.

Results

Fig. 1 shows representative examples of raw Raman spectra obtained from a series of aqueous neopentanol $(CH_3)_3CCH_2OH$, solutions ranging in concentration from 0 to 0.37 M. The broad OH band peaked at ≈3,400 cm^{-1} in all these spectra appears essentially identical to that of bulk water (Fig. 1, blue), except for the emergence of the solute's intramolecular CH stretch bands (at ≈2,900 cm^{-1}) with increasing solute concentration. The solute-correlated spectrum (Fig. 1, red), which is obtained from these input spectra by using MCR (as described in *Materials and Methods*), clearly reveals several small OH stretch features in the 3,100-cm^{-1} to 3,700-cm^{-1} frequency range. Our assignment of the narrower high-frequency peak to a water dangling OH bond arising from the hydration shell around hydrocarbon groups is supported by the following observations.

The narrow high-frequency OH peak of interest (see Fig. 1) has a frequency of ≈3,661 ± 2 cm^{-1} and a width of ≈33 cm^{-1} and thus closely resembles dangling OH stretch peaks previously observed at macroscopic air–water and oil–water interfaces (15, 18). More specifically, the dangling OH peaks at a macroscopic air–water and oil–water interfaces are centered at 3,705 ± 5 cm^{-1} and 3,674 ± 3 cm^{-1}, respectively, and have full widths of ≈40 cm^{-1} (18). Thus, dispersive (van der Waals) interactions between a water dangling OH bond and an overlying oil layer lead to a slight red-shift (relative to an air–water interface) that is comparable in magnitude to the red-shift of the OH band that we have observed in aqueous neopentanol solutions.

When water is replaced by D_2O, the frequency of the narrow solute-correlated band is decreased by the expected factor of approximately $\sqrt{2}$, whereas replacing all of the solute CH groups by CD (and by using H_2O as the solvent) leaves the frequency of

Author contributions: D.B.-A. designed research; P.N.P., K.R.F., C.L., E.J.S., and J.T.-P. performed research; P.N.P., K.R.F., E.J.S., and J.T.-P. analyzed data; and D.B.-A. wrote the paper.

The authors declare no conflict of interest.

This article is a PNAS Direct Submission.

[1]To whom correspondence should be addressed. E-mail: bendor@purdue.edu.

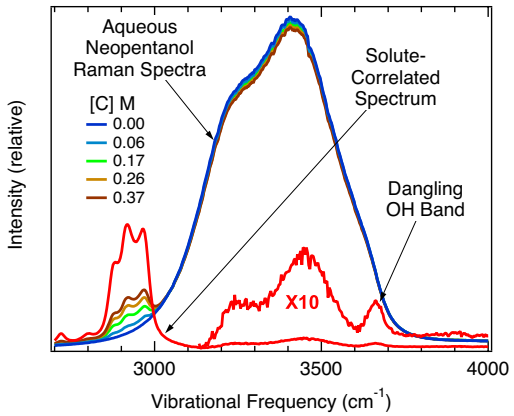

Fig. 1. The broad OH stretch band of pure water (blue), obtained by using normal (nonenhanced) Raman scattering, is shown along with the corresponding spectra of aqueous neopentanol solutions of various concentrations [C]. The input spectra are normalized to unit area and analyzed by using MCR to produce the (red) solute-correlated Raman spectrum, which reveals a narrow dangling OH peak at 3,661 ± 2 cm^{-1}.

the solute-correlated band unchanged. These results confirm that the observed solute-correlated band results from an OH stretch vibration (rather than a CH-related combination band).

Our assignment of this OH band to water, rather than the alcohol OH head group, is supported by our observation of similar solute-correlated OH bands in aqueous solutions of linear and cyclic ethers, diethyl ether $CH_3CH_2OCH_2CH_3$ and tetrahydrofuran c-$(CH_2)_4O$ (which reveal narrow OH peaks at ≈3,663 cm^{-1} and ≈3,664 cm^{-1}, respectively). Moreover, experiments performed by using a series of linear, branched and cyclic alcohols indicate that the intensity of the dangling OH band generally increases with alkane size (as shown in Fig. 2 and described below). This correlation further supports our conclusion that the dangling OH feature we have observed derives from

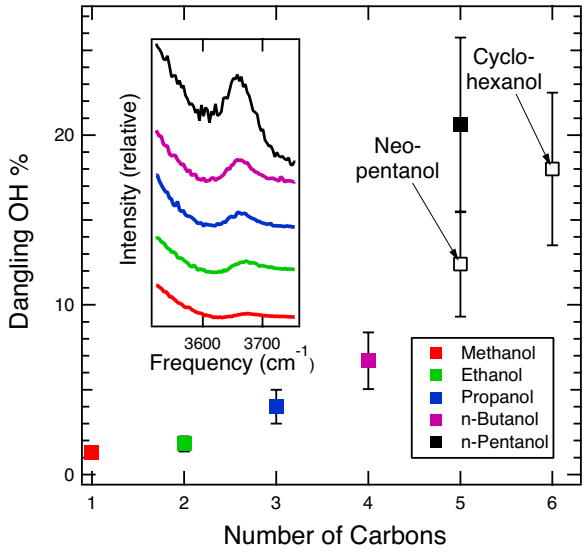

Fig. 2. The intensities of the water dangling OH bands obtained from various aqueous alcohol (hydroxylated alkane) solutions. The *Inset* shows the relative intensities of the experimental (Raman-MCR) dangling OH band obtained from *N*-alcohol solutions. The points represent the corresponding dangling OH concentrations expressed as the probability (dangling OH %) of observing an OH bond in the hydration shell around the corresponding alkane groups (see *Materials and Methods* for further details).

hydration-shell water molecules, rather than from the alcohol OH head group.

The areas of the dangling OH peaks are found to scale approximately linearly with solute concentration, confirming that the dangling OH bonds are associated with isolated alkane chains rather than aggregates consisting of 2 or more solutes. Our observation of dangling OH bonds around solutes as small as methanol (see dangling OH spectra in Fig. 2 *Inset*) clearly implies that liquid water does not form perfect clathrate–hydrate structures around small nonpolar groups. The integrated area of the dangling OH peak obtained from aqueous n-butanol is very similar to that observed around diethyl ether and tetrahydrofuran (of the same concentration). This implies that dangling OH bond formation is relatively insensitive to the secondary (conformational) structure of short alkane chains, because the latter 3 solutes all have 4 methyl (or methylene) groups. On the other hands, the number of dangling OH bonds around neopentanol is approximately half that around *N*-pentanol (as shown in Fig. 2), which implies that branching of longer-chain alkanes tends to decrease the dangling OH formation probability. This conclusion is further supported by our observation that cyclohexanol induces approximately the same number of water dangling OH bonds as n-pentanol.* Moreover, our results pertaining to a series of n-alcohols (solid points in Fig. 2) suggest that there is a sharp increase in the dangling OH formation probability (OH %) between n-butanol and n-pentanol (whose potential significance is further discussed below).

Previous studies have suggested that the OH stretch frequency shifts of water molecules in pure liquid water and aqueous solutions are primarily dictated by the electric field (Stark shift) experienced by each OH group (21–23). We have used the previously determined correlation between electric field strength and OH vibrational frequency (22) to simulate the OH stretch spectral features arising from the hydration shell around alkane and aromatic solutes (see *Materials and Methods* for further details). The results shown in Fig. 3 *A–C* compare the dangling OH bands obtained from aqueous neopentane (red) and benzene (green) simulations with the corresponding experimental (Fig. 3*D*) Raman-MCR results for aqueous neopentanol (red) and benzyl alcohol (green). Note in particular the remarkably close agreement between the frequencies of the simulated and experimental dangling OH bands in Fig. 3 *C* and *D*, respectively. However, the number of water dangling OH bonds (per solute) that are obtained from the simulation results are somewhat larger than the corresponding experimentally derived values. More specifically, the simulations imply that there are ≈2 dangling (π-H bonded) OH bonds around benzene and ≈1 dangling OH bond around neopentane (which would correspond to dangling OH probabilities of OH % ≈200% and 100%, respectively). The experimental dangling OH band intensities, on the other hand, suggest somewhat lower dangling OH probabilities of OH% ≈74% (±19%) around benzyl alcohol and ≈12% (±4%) around neopentanol (obtained as further described in *Materials and Methods*).

The 30- to 40-cm^{-1} width of the dangling OH peaks that we have observed (as well as those at air–water and oil–water interfaces) implies that the corresponding water structure has a lifetime of at least 0.2 ps. More specifically, the dangling OH lifetime must be $>1/(2\pi cy)$, where γ is the full width at half-maximum of the dynamic (Lorenzian) contribution to the dangling OH band width (where c is the speed of light). In other words, if the dangling OH bond was significantly shorter-lived

*Although the solubility of n-hexanol is too low (≈0.06 M) to allow accurate dangling OH intensity measurements using the present Raman-MCR method, if we assume the number of dangling OH bonds around n-hexanol is larger than that around n-pentanol, then our aqueous cyclohexanol results imply that cyclization suppress dangling OH bond formation.

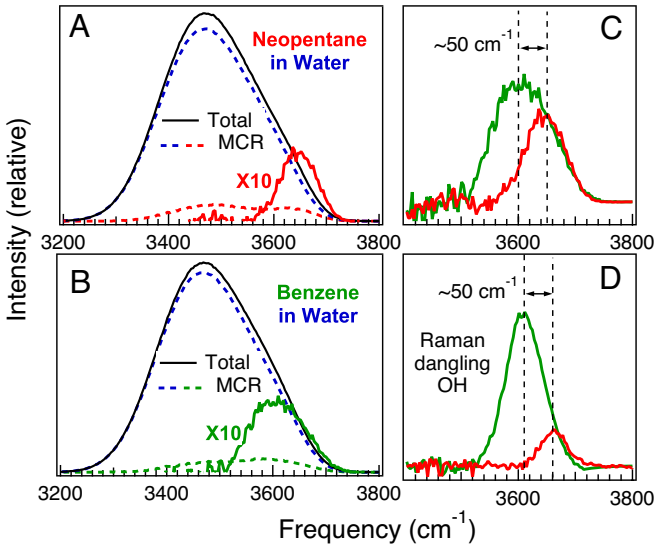

Fig. 3. Comparison of simulated and experimental dangling OH vibrational bands. (*A* and *B*) Computer simulations of the electric field strengths experienced by water OH groups in aqueous neopentane ($(CH_3)_4C$ (*A*), and benzene C_6H_6 (*B*), solutions are used to predict the corresponding OH vibrational band shapes (solid black curves). The dashed curves in *A* and *B* show the corresponding bulk water (blue) and solute-correlated (red or green) MCR components obtained at a solute concentration of 0.77 M. (*C* and *D*) The resulting dangling OH features (*C*) around neopentane (red) and benzene (green) are compared with the corresponding experimental (*D*) dangling OH bands in neopentanol (red) and benzyl alcohol $C_6H_5CH_2OH$ (green), as further described in *Results* and *Materials and Methods*.

than 0.2 ps, then the associated vibrational peak would necessarily be broader than the observed peak. This lower bound is physically reasonable because it is significantly shorter than the >2.5-ps rotational reorientation time of a water molecule in the hydration shell around nonpolar groups, as observed by using both infrared pump probe (4, 24) and NMR (5) experiments. Moreover, 0.2 ps is much shorter than the ≈200-ps vibrational relaxation time of dangling OH bonds at nano–bubble interfaces in liquid water, as measured by using incoherent anti-Stokes Raman pump-probe spectroscopy (25). More generally, both experimental and theoretical studies confirm that interfacial water molecules typically both rotationally and vibrationally relax more slowly than bulk water (6, 26, 27). Thus, the actual lifetime of the dangling OH bonds that we have observed may well be much longer than the 0.2-ps lower bound imposed by the width of the dangling OH peak.

The frequency of the dangling OH bands that we have observed in the hydration shells around alkane groups are invariably ≈40 ± 5 cm^{-1} red-shifted (lower in frequency) than those of dangling OH bonds at the air–water interface (18). This red-shift may be used to obtain an estimate of the force that a dissolved hydrocarbon group exerts on a water dangling OH bond. We have estimated this force using a theoretical expression first derived by David Buckingham (28, 29) (as further described in *Materials and Methods*). The results indicate that dispersive (van der Waals) interactions between the water dangling OH and the solute alkane group produces an extensional force of ≈0.3 nN on the dangling OH group (relative to a dangling OH group at an air–water interface). The additional 50-cm^{-1} red-shift of the dangling OH bond around benzyl alcohol (see Fig. 3) implies that the phenyl group induces a total force of ≈0.7 nN on the associated water OH group. It is also noteworthy that the latter 50-cm^{-1} frequency shift is similar to the 60- to 70-cm^{-1} difference between free OH and π-H-bonded OH groups in low-temperature benzene–water clusters (30). Thus, our results may represent experimental evidence of the formation of a π-H bond in liquid water.

Conclusions

Although the discovery of water dangling OH bonds in aqueous solutions containing hydrocarbon groups is surprising, it is certainly not physically unreasonable. There is ample reason to question the traditional view that water forms perfect clathrate–hydrate structures around small hydrocarbon groups (3). Even if one allows for some residual resemblance between solid clathrate–hydrate structures and the hydration shells around small nonpolar solutes in liquid water, it is certainly not reasonable to expect the latter structures to be free of defects. The fact that we have observed dangling OH bonds in aqueous solutions containing hydrocarbon groups clearly confirms the presence of such defects. Moreover, we have used the width and frequency of the observed OH stretch peaks to place a lower bound on the lifetime of the associated dangling OH structures as well as to estimate the mean force experienced by the dangling OH groups (relative to a dangling OH at a macroscopic air–water interface).

Geometric constraints imposed by the low curvature of macroscopic air–water and oil–water interfaces require the formation of water dangling OH bonds. Our observation of dangling OH bonds in the hydration shells around dissolved hydrocarbon groups confirms that dangling OH bonds are also present at such higher curvature interfaces. However, the probability of forming a dangling OH bond (per unit interfacial area), is clearly much smaller in the hydration shells around hydrocarbon solutes than at macroscopic interfaces. More specifically, at an air–water interface, ≈1 in 4 water molecules contain a dangling OH group (15). In contrast, our results indicate that only ≈1 of 1,000 water molecules in the hydration shell around a dissolved ethanol molecule form a dangling OH group.[†] Thus, although dangling OH bonds are found at both macroscopic and molecular hydrophobic interfaces, the probability of forming a dangling OH clearly decreases significantly as the curvature of the interface increases.

One of the most intriguing aspects of our results is the nonlinear increase in the dangling OH probability shown in Fig. 2, and particularly the sharp increase between n-butanol and n-pentanol. Because the excluded surface area of n-alkane groups is nominally a linear function of solute chain length,[‡] the clearly nonlinear chain length dependence of the n-alcohol results in Fig. 2 thus indicates that dangling OH formation is not simply proportional to water-accessible surface area. Moreover, our results indicate that branching (or cyclization) has the effect of suppressing dangling OH bond formation. Interestingly, the largest experimentally observed cavities formed in solid hydrocarbon–water clathrate-hydrates approximately correspond with the size of neopentane (31). Moreover, this size is also approximately the same as that at which dewetting around idealized hydrophobic particles begins to occur (7, 32, 33). Thus, our observation of a sharp increase in the formation of dangling OH bonds around n-pentanol may indicate the onset of the collective breaking of water hydrogen bonds around large hydrocarbon groups.

On the other hand, our simulated dangling OH spectra do not reproduce the experimentally observed nonlinear chain length dependence (and marked influence of branching), but rather are

[†]This estimate is obtained from our observation that ≈2% of the dissolved ethanol molecules give rise to a single water dangling OH bond, combined with the fact there are ≈20 water molecules in the first hydration-shell around ethanol's CH_3CH_2- group.

[‡]The water excluded surface area would be strictly a linear function of chain length for rigid (all-*trans*) chains, but would be expected to have a slightly negative, sub-linear, curvature for flexible chains.

consistent with an approximately linear surface area correlation of the dangling OH bond formation. However, given the reproducibility of our experimental results, we are inclined to attribute the discrepancies between our experimental and simulated dangling OH formation probabilities to limitations of the TIP4P water model and/or the electric field correlation strategy used to predict water OH spectra. It will clearly be interesting to extend the above studies to other aqueous solutions and more accurate vibrational frequency simulations, as well as variable temperature (and pressure) studies.

Materials and Methods

Experiments. Raman spectra of aqueous solutions ranging in concentration from 0 to 5 wt % (or 0–1 M) are decomposed into bulk water and solute-correlated components by using MCR (19, 20). The resulting solute-correlated spectra contain features arising both from the solute itself and from water molecules whose vibrational spectra are significantly perturbed by the solute, including the well-resolved high-frequency OH features that are the focus of the present work.

Because the OH feature of interest is ≈100–1,000 times weaker than the overlying broad OH stretch band of bulk water, as shown in Fig. 1, observing the dangling OH band requires collecting input Raman spectra with a signal-to-noise ratio of the order of 1,000:1 and little or no background (e.g., fluorescence) interference. Thus, we employ solutes (and water) of the highest available grade of purity and distill these as needed to further reduce any residual fluorescence background. Raman spectra were obtained by using an Ar-ion excitation laser (of 514.5-nm wavelength with ≈50-mW power at the sample) and a home-built microRaman system (34). Each Raman spectrum was integrated for a total of 400 s. Pairs of identically collected spectra were compared in order to identify and remove cosmic spike artifacts (35) before MCR analysis.

Dangling OH probabilities are obtained by first determining the Raman area of the OH band of pure water (divided by twice the concentration of water) and that of the CH band of the solute dissolved in water (divided by the solute concentration). The ratio of these areas represents the ratio of the effective Raman cross-sections of water, per OH group, to that of the solute CH band. This Raman cross-section ratio, combined with the relative areas of the CH and dangling OH bands in each solute-correlated spectrum is used to estimate the number water dangling OH bonds associated with each solute molecule. This estimate implicitly assumes that the Raman cross-section of a water OH group is constant (and equal to that in bulk water), which is undoubtedly not exactly correct. However, our comparisons of OH band areas in other systems (as described below) suggest that the resulting dangling OH probabilities are accurate to within a factor of 2 (and may readily be refined by using future theoretical or experimental determinations of the Raman cross-section of water dangling OH bonds).

The Raman intensity of an OH group is approximately half that of a water molecule, as determined by comparing the Raman band areas of 1 M HOD in D_2O with that of pure H_2O divided by 111 M (which is the molarity of the OH groups in water at ambient pressure and temperature). More specifically, the difference between the resulting OH band areas (after dividing by the OH concentration) suggest that the Raman cross-section of a localized OH vibration in HOD (dissolved in D_2O) may be slightly smaller (by less than ≈15%) than that of a resonantly coupled OH in H_2O (dissolved in H_2O). Moreover, Raman measurements of small amounts (5–10 wt %) of water dissolved in either THF or pyridine suggest that the Raman cross-section of water surrounded by these organic solvents is again somewhat smaller than that of bulk water (by between 30% and 50%). These results suggest that the Raman cross-section of a dangling OH bond in the hydration shell around a dissolved hydrocarbon group may be as much as a factor of 2 smaller than that of an OH bond in bulk water. Thus, our estimated dangling OH percentage values plotted in Fig. 2 may underestimate the true dangling OH concentrations by up to a factor of 2.

Simulations. Molecular dynamics simulations at constant temperature and pressure were performed on systems containing a single hydrocarbon solute molecule and 500 TIP4P water molecules (at a temperature of 300 K and a pressure of 0.1 MPa with a step size of 1 fs and a duration of 10 ns after a total of 65 ps equilibration). Electric field distributions were obtained by determining the electric field strength at each water H atom (directed along the OH bond) in 10^5 solution configurations, sampled every 100 fs (and sorted into electric field strength bins of 2×10^8 V/m width). These electric field distributions were converted to vibrational frequency predictions by using the same expression used by Smith, Saykally, and Geissler (22) to predict water OH Raman band shapes in aqueous alkali halide salt solutions. In particular, the simulated electric field strengths (E) were converted to OH vibrational (Raman shift) band frequencies by using $\omega\ (\mathrm{cm}^{-1}) = 3{,}745 - 16.0514 \times 10^{-9} \cdot \mathrm{E(V/m)}$.

Simulation results pertaining to solutions of various concentrations were approximated by considering water molecules contained within spheres of different radii around the solute (ranging from 6 to 10 Å from the center of each solute). The corresponding solute concentration is obtained by dividing the number of solutes (one) by the volume of each sphere, to yield solute concentrations ranging from 0.4 M to 1.8 M (as the sphere radius ranges from 10 Å down to 6 Å). The resulting simulated OH stretch spectra were analyzed by using the same MCR procedure that is used to analyze the experimental Raman spectra.

The black curves in Fig. 3 *A* and *B* show the OH stretch band obtained from water electric field distributions, and the dashed curves show the corresponding MCR bulk water (blue) and solute-correlated (colored) components. The narrow high-frequency OH (solid colored) bands shown in Fig. 3 *A–D* are obtained after subtracting the lower frequency contributions to the corresponding solute-correlated OH spectra. The latter subtractions are performed by using either a shifted and scaled copy of the pure water MCR component (in the case of the electric field derived spectra) or a Gaussian fit to the lower-frequency OH band in the solute-correlated MCR spectrum (in the case of the experimental spectra).

Intermolecular Force Measurements. The force along a dangling OH bond was estimated by using the following expression for the solvent mean force along a pseudodiatomic bond (28, 29, 36, 37): $F \approx [-2f^2/(3g)](\Delta\omega/\omega)$. The ratio $\Delta\omega/\omega$ represents the frequency shift of the dangling OH relative to that at the air–water interface, whereas $f \approx 918$ nN/nm and $g \approx -19{,}600$ nN/nm^2 are the harmonic and anharmonic force constants, respectively, of a localized (isolated) OH stretching vibration. More specifically, the latter force constants were obtained from MP2/6-311++G(d,p) quantum calculations of the change in the ground-state energy of an isolated water molecule when one of its OH bonds is stretched about the potential minimum, and fit to a cubic polynomial, $U(r) = \frac{1}{2}f(\Delta r)^2 + \frac{1}{2}g(\Delta r)^3$ (where $\Delta r = r - r_{\mathrm{min}}$).

ACKNOWLEDGMENTS. We thank David Chandler and Steve Granick for insightful comments and Alexander C. Davis for performing the quantum calculations that we used to estimate the harmonic and anharmonic force constants for a water OH stretch vibration. This work was supported by the National Science Foundation.

1. Tanford C (1978) Hydrophobic effect and organization of living matter. *Science* 200:1012–1018.
2. Frank HS, Evans JW (1945) Free volume and entropy in condensed systems. 3. Entropy in binary liquid mixtures; partial molar entropy in dilute solutions; structure and thermodynamics of aqueous electrolytes. *J Chem Phys* 13:507.
3. Ashbaugh HS, Asthagiri D, Pratt LR, Rempe SB (2003) Hydration of krypton and consideration of clathrate models of hydrophobic effects from the perspective of quasi-chemical theory. *Biophys Chem* 105:323–338.
4. Rezus YLA, Bakker HJ (2007) Observation of immobilized water molecules around hydrophobic groups. *Phys Rev Lett* 99:148301.
5. Qvist J, Halle B (2008) Thermal signature of hydrophobic hydration dynamics. *J Am Chem Soc* 130:10345–10353.
6. Laage D, Stirnemann G, Hynes JT (2009) Why water reorientation slows without iceberg formation around hydrophobic solutes. *J Phys Chem B* 113:2428–2435.
7. Lum K, Chandler D, Weeks JD (1999) Hydrophobicity at small and large length scales. *J Phys Chem B* 103:4570–4577.
8. Chandler D (2005) Interfaces and the driving force of hydrophobic assembly. *Nature* 437:640–647.
9. Zhou R, Huang X, Margulis CJ, Berne BJ (2004) Hydrophobic collapse in multidomain protein folding. *Science* 305:1605–1609.
10. Giovambattista N, Lopez CF, Rossky PJ, Debenedetti PG (2008) Hydrophobicity of protein surfaces: Separating geometry from chemistry. *Proc Natl Acad Sci USA* 105:2274–2279.
11. Ashbaugh HS, Pratt LR, Paulaitis ME, Clohecy J, Beck TL (2005) Deblurred observation of the molecular structure of an oil–water interface. *J Am Chem Soc* 127:2808–2809.
12. Qvist J, Davidovic M, Hamelberg D, Halle B (2008) A dry ligand-binding cavity in a solvated protein. *Proc Natl Acad Sci USA* 105:6296–6301.
13. Zhang XY, Zhu YX, Granick S (2002) Hydrophobicity at a Janus interface. *Science* 295:663–666.
14. Athawale MV, Goel G, Ghosh T, Truskett TM, Garde S (2007) Effects of lengthscales and attractions on the collapse of hydrophobic polymers in water. *Proc Natl Acad Sci USA* 104:733–738.
15. Du Q, Freysz E, Shen YR (1994) Surface vib spectroscopic studies of hydrogen-bonding and hydrophobicity. *Science* 264:826–828.

16. Ji N, Ostroverkhov V, Tian CS, Shen YR (2008) Characterization of vibrational resonances of water–vapor interfaces by phase-sensitive sum-frequency spectroscopy. *Phys Rev Lett* 100:096102:1–4.
17. Scatena LF, Brown MG, Richmond GL (2001) Water at hydrophobic surfaces: Weak hydrogen bonding and strong orientation effects. *Science* 292:908–912.
18. Moore FG, Richmond GL (2008) Integration or segregation: How do molecules behave at oil/water interfaces? *Acc Chem Res* 41:739–748.
19. de Juan A, Tauler R (2006) Multivariate curve resolution (MCR) from 2000: Progress in concepts and applications. *Crit Rev Anal Chem* 36:163–176.
20. Perera P, Wyche M, Loethen Y, Ben-Amotz D (2008) Solute-induced perturbations of solvent-shell molecules observed using multivariate Raman curve resolution. *J Am Chem Soc* 130:4576–4579.
21. Fecko CJ, Eaves JD, Loparo JJ, Tokmakoff A, Geissler PL (2003) Ultrafast hydrogen-bond dynamics in the infrared spectroscopy of water. *Science* 301:1698–1702.
22. Smith JD, Saykally RJ, Geissler PL (2007) The effects of dissolved halide anions on hydrogen bonding in liquid water. *J Am Chem Soc* 129:13847–13856.
23. Corcelli SA, Skinner JL (2005) Infrared and Raman line shapes of dilute HOD in liquid H_2O and D_2O from 10 to 90 degrees C. *J Phys Chem A* 109:6154–6165.
24. Rezus YLA, Bakker HJ (2008) Femtosecond spectroscopic study of the solvation of amphiphilic molecules by water. *Chem Phys* 350:87–93.
25. Wang ZH, Pang Y, Dlott DD (2006) Long-lived interfacial vibrations of water. *J Phys Chem B* 110:20115–20117.
26. Zhao W, Moilanen DE, Fenn EE, Fayer MD (2008) Water at the surfaces of aligned phospholipid multibilayer model membranes probed with ultrafast vibrational spectroscopy. *J Am Chem Soc* 130:13927–13937.
27. Harpham MR, Levinger NE, Ladanyi BM (2008) An investigation of water dynamics in binary mixtures of water and dimethyl sulfoxide. *J Phys Chem B* 112:283–293.
28. Melendez-Pagan Y, Ben-Amotz D (2000) Intermolecular forces and bond length changes in high-pressure fluids. Vibrational spectroscopic measurement and generalized perturbed hard fluid analysis. *J Phys Chem B* 104:7858–7866.
29. Hutchinson EJ, Ben-Amotz D (1998) Molecular force measurement in liquids and solids using vibrational spectroscopy. *J Phys Chem B* 102:3354–3362.
30. Gruenloh CJ, et al. (1997) Infrared spectrum of a molecular ice cube: The S-4 and D-2d water octamers in benzene-(water)(8). *Science* 276:1678–1681.
31. Sloan ED (1998) *Clathrate Hydrates of Natural Gases* (Marcel Dekker, New York).
32. Stillinger FH (1973) Structure in aqueous solutions of nonpolar solutes from the standpoint of scaled-particle theory. *J Solut Chem* 2:141–158.
33. Huang X, Margulis CJ, Berne BJ (2003) Do molecules as small as neopentane induce a hydrophobic response similar to that of large hydrophobic surfaces? *J Phys Chem B* 107:11742–11748.
34. Zhang DM, Ortiz C, Xie Y, Davisson VJ, Ben-Amotz D (2005) Detection of the site of phosphorylation in a peptide using Raman spectroscopy and partial least squares discriminant analysis. *Spectroc Acta A* 61:471–475.
35. Zhang DM, Jallad KN, Ben-Amotz D (2001) Stripping of cosmic spike spectral artifacts using a new upper-bound spectrum algorithm. *Appl Spectrosc* 55:1523–1531.
36. Buckingham AD (1960) Solvent effects in vib spectrosc (1960) *Trans Faraday Soc* 56:753–760.
37. Buckingham AD (1958) solvent effects in infra-red spectroscopy. *Proc R Soc London Ser A* 248:169–182.